ATM and ATR Influence Meiotic Crossover Formation Through Antagonistic and Overlapping Functions in *Caenorhabditis elegans*

Wei Li*,† and Judith L. Yanowitz*,1

*Magee-Womens Research Institute, Department of Obstetrics, Gynecology, and Reproductive Sciences, University of Pittsburgh School of Medicine, Pennsylvania 15213 and †Tsinghua University MD Program, School of Medicine, Tsinghua University, Haidian District, Beijing 100084, PR China

ORCID ID: 0000-0001-6886-8787 (J.L.Y.)

ABSTRACT During meiosis, formation of double-strand breaks (DSBs) and repair by homologous recombination between homologs creates crossovers (COs) that facilitate chromosome segregation. CO formation is tightly regulated to ensure the integrity of this process. The DNA damage response kinases, Ataxia-telangiectasia mutated (ATM) and RAD3-related (ATR) have emerged as key regulators of CO formation in yeast, flies, and mice, influencing DSB formation, repair pathway choice, and cell cycle progression. The molecular networks that ATM and ATR influence during meiosis are still being resolved in other organisms. Here, we show that *Caenorhabditis elegans* ATM and ATR homologs, ATM-1 and ATL-1 respectively, act at multiple steps in CO formation to ultimately ensure that COs are formed on all chromosomes. We show a role for ATM-1 in regulating the choice of repair template, biasing use of the homologous chromosome instead of the sister chromatid. Our data suggest a model in which ATM-1 and ATL-1 have antagonistic roles in very early repair processing, but are redundantly required for accumulation of the RAD-51 recombinase at DSB sites. We propose that these features of ATM-1 and ATL-1 ensure both CO formation on all chromosomes and accurate repair of additional DSBs.

KEYWORDS ATM; ATR; meiosis; *C. elegans*; DSB repair

CROSSOVER (CO) recombination—the exchange of DNA between homologous chromosomes—occurs in meiosis I and is a key step to ensure that chromosomes are segregated properly. Many factors contribute to the recombination outcome, including the number of double-strand breaks (DSBs) made during meiosis, their distribution, and the repair pathway chosen following the formation of DSBs. The formation and repair of DSBs and the conversion of some of these into COs is a highly regulated process that must be tightly controlled to ensure the proper subsequent segregation of chromosomes. Mechanisms have evolved to tune DSB numbers to species-specific levels (Gray *et al.* 2013), and also to channel a limited number of DSBs into COs (Martini *et al.* 2006).

The DNA damage response (DDR) kinases ATM/Tel1 (ataxia-telangiectasia mutated) and ATR/Mec1 (ataxia-telangiectasia and RAD-3 related) have emerged as key conserved players in CO homeostasis (reviewed in MacQueen and Hochwagen(2011; Cooper *et al.* 2014). ATM mutations lead to severe meiotic defects and infertility in mice, yeast, and flies (Barlow *et al.* 1996, 1998; Xu *et al.* 1996). ATM both downregulates Spo11-mediated DSBs (Joyce *et al.* 2011; Lange *et al.* 2011; Zhang *et al.* 2011; Carballo *et al.* 2013; Garcia *et al.* 2015) and affects their distribution (Zhang *et al.* 2011; Anderson *et al.* 2015; Garcia *et al.* 2015). It also biases use of the homolog as a repair template [interhomolog homologous recombination (IH-HR)] *vs.* the sister chromatid [intersister (IS-HR)]. ATR, by contrast, positively regulates DSB formation (Gray *et al.* 2013). Together, ATM and ATR establish a regulatory feedback through the phosphorylation of components of the DSB machinery and chromatin axes (Cooper *et al.* 2014). Although yeast ATM and ATR (Tel1

doi: https://doi.org/10.1534/genetics.119.302193
Manuscript received March 12, 2019; accepted for publication April 14, 2019; published Early Online April 23, 2019.
Supplemental material available at FigShare: https://doi.org/10.25386/genetics.7973795.
[1]Corresponding author: Magee-Womens Research Institute, Department of Obstetrics, Gynecology, and Reproductive Sciences, University of Pittsburgh School of Medicine, 204 Craft Ave., Rm. A224, Pittsburgh, PA 15213. E-mail: yanowitzjl@mwri.magee.edu

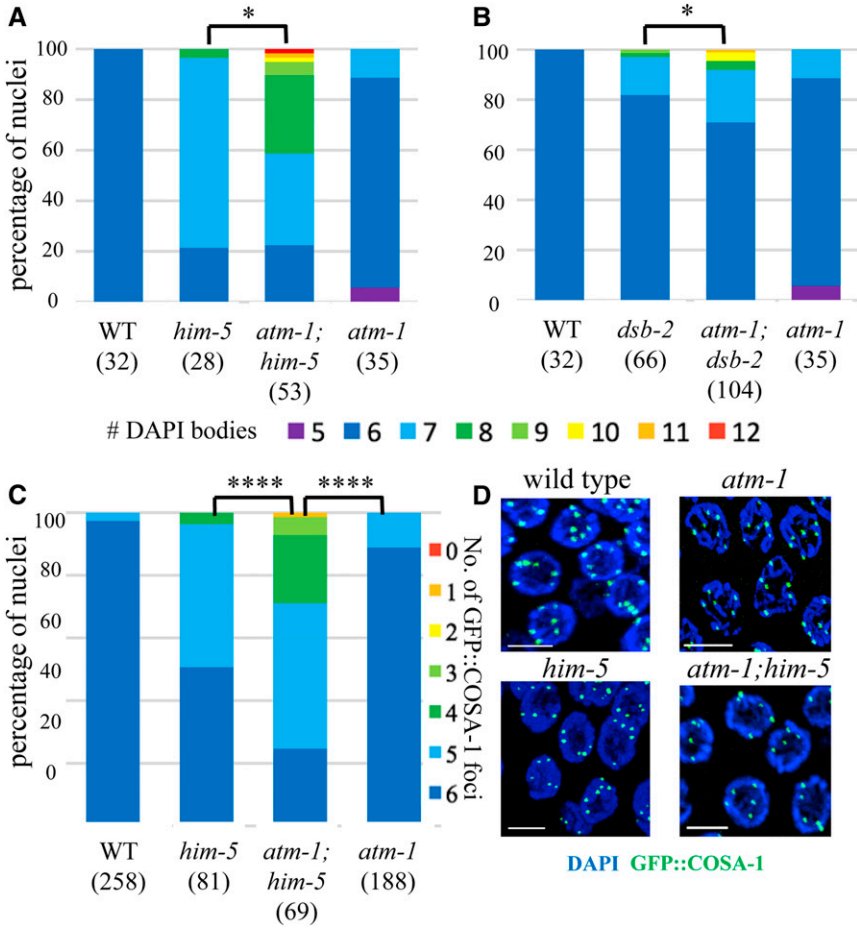

Figure 1 *atm-1* mutations exacerbate CO defects of DSB-defective mutants: *him-5* and *dsb-2*. (A, B) Quantification of DAPI bodies in −1 nuclei; *$P < 0.05$, two-tailed Mann-Whitney test. (C) Proportion of nuclei with indicated numbers of GFP::COSA-1 foci. **** $P < 0.0001$, two-tailed Mann-Whitney test. Three gonads were analyzed for each genotype. Numbers below each genotype indicate the numbers of nuclei analyzed. (D) Images of *him-5* and *atm-1;him-5* late pachytene nuclei are shown with DAPI (blue) and GFP::COSA-1 (green). Bar, 5 μm.

and Mec1, respectively) seem to function antagonistically to enforce DSB homeostasis, the interplay between the two genes and their functions in CO formation are more complex. For example, research in yeast supports that there is a DSB threshold above which Tel1 plays a role (with Pch2 and Mec1) in homolog bias, while, with low-abundance DSBs, Tel1 promotes resection (Joshi *et al.* 2015; Mimitou *et al.* 2017). Thus, further insights into the functional consequences of ATM/ATR loss on CO formation through the analysis of additional model systems may help provide new insights into ATM/ATR function.

In *Caenorhabditis elegans*, the orthologs of ATM and ATR, ATM-1 and ATL-1 (ATM-like), are required for genome stability (Jones *et al.* 2012). In addition, more RAD-51 foci were observed in meiotic cells in *atm-1* mutants compared to wild type—a result that was consistent with a conserved role in DSB inhibition (Checchi *et al.* 2014). However, further information about the role of ATM-1 in DSB and CO formation remains unknown. Loss of *atm-1* function has been reported to lead to a mild increase in meiotic nondisjunction, suggesting a more complex relationship between DSB formation and CO induction. Because most chromosomes receive a single CO each meiosis (high CO interference), and because only a single CO pathway has been identified in *C. elegans*, we reasoned that the worm offered an opportunity to investigate both conserved features of ATM and ATR functions in meiosis and to dissect out their contributions to unique aspects of CO control that are harder to examine in other systems. Here, we show that *C. elegans atm-1* and *atl-1* act at multiple steps in CO formation to ultimately ensure that COs are formed on all chromosomes.

Materials and Methods

Genetics and worm handling

All strains were grown and maintained at 20° on standard media (Brenner 1974). Mutant strains used in this study were: LGI *atm-1(gk186)*, *rad-54(ok615)*; LGII *dsb-2(me96)*, *smc-5(ok2421)*; *meIs8[unc-119(+) pie-1promoter::gfp::cosa-1]*; LGIII *brc-1(tm1145)*, *dpy-18(e364)*, *unc-64(e246)*, *dpy-1(e1)*, *lon-1(e185)*; LGIV *spo-11(me44)*, *dsb-1(we11)*; LGV *him-5(ok1896)*, *syp-1(me17)*, *atl-1(tm853)*. *atm-1(gk186)* is a deletion allele that removed upstream promoter sequences and half of the 5′ coding sequence; it is a presumptive null. *atl-1(tm853)* is an ~700 bp deletion in the coding sequence that is a strong loss-of-function or null. Some strains were provided by the *Caenorhabditis* Genetics Center, which is funded by National Institutes of Health, Office of Research Infrastructure Programs (P40 OD010440). Double, triple, and quadruple mutants were generated using

Table 1 *ATM-1* mutants exacerbate defects in recombination

Genotype	N2	*atm-1*	*him-5*	*atm-1;him-5*
		dpy-18 (III: 8.85), *unc-64* (III: 21.20)		
Recombination rate	12.01% (1896)	11.97% (2816)	14.22%,#(2475)	10.93% ***(1587)
		dpy-1 (III: −15.66), *lon-1* (III: −1.63)		
Recombination rate	17.56% (3995)	15.99% (1958)	17.14%*** (2705)	13.78%*** (1652)

Chi square test, #N2 *vs. him-5*, $P < 0.05$; ***him-5 vs. atm-1;him-5*, $P < 0.0001$. All other comparisons, n.s.

standard genetic techniques with PCR verification of genotypes, and are listed in Supplemental Material, Table S1.

Immunofluorescence

Adult worms were dissected in 1× sperm salts with 1 mM levamisole, and fixed in 2% paraformaldehyde/1× PBS for 5 min in a humid chamber. Slides were then freeze-cracked and immersed in 100% ethanol for 2 min followed by 5 sec in acetone. Slides were then washed in PBSTB [1× PBS with 0.1% Tween and 0.1% bovine serum albumin (BSA)], and incubated overnight at 4° in primary antibody (rabbit anti-RAD-51, 1:30,000, gift from S. Smolikove, rabbit anti-DSB-2, 1:20,000, gift from A. Villeneuve) diluted in PBSTB. The next day, slides were washed 3× in PBSTB and incubated in secondary antibody (α-rabbit Alexa 568, 1:2000) for 4 hr at room temperature in the dark. Then slides were washed 2× 10 min, and stained 1× 10 min with DAPI (10 mg/ml stock diluted 1:50,000 in 1× PBS). Slides were mounted in Prolong Gold with DAPI and put in the dark to dry overnight before imaging.

Analysis of RAD-51 foci

Three-dimensional (3D) images of the whole germ lines were taken using a Nikon A1r confocal microscope and analyzed using Volocity 3D software (PerkinElmer). For wild type and *atm-1*, *him-5*, *dsb-2*, *atm-1;him-5* and *atm-1;dsb-2* mutants, as well as irradiated and nonirradiated *spo-11* mutants and *atm-1;spo-11*, we divided the pachytene region into six zones, and counted RAD-51 foci in every nucleus for a minimum of three germ lines/genotype. For *rad-54;him-5* mutants and *atm-1;rad-54;him-5* mutants, we counted the RAD-51 foci in late pachytene nuclei for at least three germ lines/genotype. For analysis of *atl-1* mutants (Figure 7 and Figure 8), the transition zone (TZ) was included and the pachytene zones were binned into three regions (1 + 2)/zone (3 + 4)/zone (5 + 6) as shown in Figure 2A. Three gonad arms were analyzed/genotype.

Irradiation

Day 1 adult worms were exposed to γ-irradiation from a ^{137}Cs source (Gammacell1000 Elite; Nordion International). Dosages are described below. For analysis of diakinesis stage nuclei post-irradiation (post-IR), animals were fixed and stained 27 hr post-IR (McClendon *et al.* 2016). For the worms used for RAD-51 staining for time course analysis, we stained them 1, 2, 4, and 8 hr post-IR.

Recombination analysis

Recombination rates between *dpy-18* and unc-*64* or *dpy-1* and *lon-1* were attained by crossing the marker mutations into the respective genetic background and assaying for Dpy non-Unc and Unc-nonDpy progeny from *dpy-18 unc-64/+* parents or Lon non-Dpy (Dpy is epistatic to Lon, so cannot be assessed for recombination). More than 1000 progeny for each phenotype were analyzed, and the recombination rate was calculated based on prior results (Brenner 1974).

Analysis of GFP::COSA-1 foci

Day 1 adult worms were dissected in 2× sperm salts as described above. Slides were immediately freeze-cracked and immersed in 100% ethanol for 10 sec, and fixed in 2% paraformaldehyde/1× PBS again for 10 min. Slides were washed 2× 5 min in PBSTB, stained with DAPI in 1× PBS for 10 min followed by one wash with PBSTB for 5 min. Slides were mounted in Prolong Gold with DAPI. Images were acquired and analyzed as described above. GFP::COSA-1 foci in late pachytene nuclei were counted in at least five germ lines/genotype in the late pachytene.

Data availability

Strains and plasmids are available upon request. The authors affirm that all data necessary for confirming the conclusions of the article are present within the article, figures, and tables.

Table S1. List of strains generated for this study.

Figure S1. ATM-1 limits the accumulation of RAD-51 foci.

Figure S2. The impact of *atm-1* on non-CO outcomes is independent of SPO-11 induced breaks.

Figure S3. SPO-11-independent COs are induced in *atm-1* mutants, revealing carry-through damage from premeiotic events or meiotic S phase. At the same time, exposure to IR leads to fewer COs in *atm-1* mutant background, revealing a defect in converting DSBs to COs in the absence of ATM-1 function.

Figure S4. RAD-51 analysis in *atl-1* mutants and post-IR exposure.

Figure S5. Bioinformatic analysis of potential ATM-1/ATL-1 phosphorylation sites in *C. elegans* DSB proteins.

Supplemental material available at FigShare: https://doi.org/10.25386/genetics.7973795.

Results

ATM-1 helps promote CO formation

Meiotic DSBs are catalyzed by the conserved topoisomerase SPO11. SPO11 activity is regulated by accessory factors that

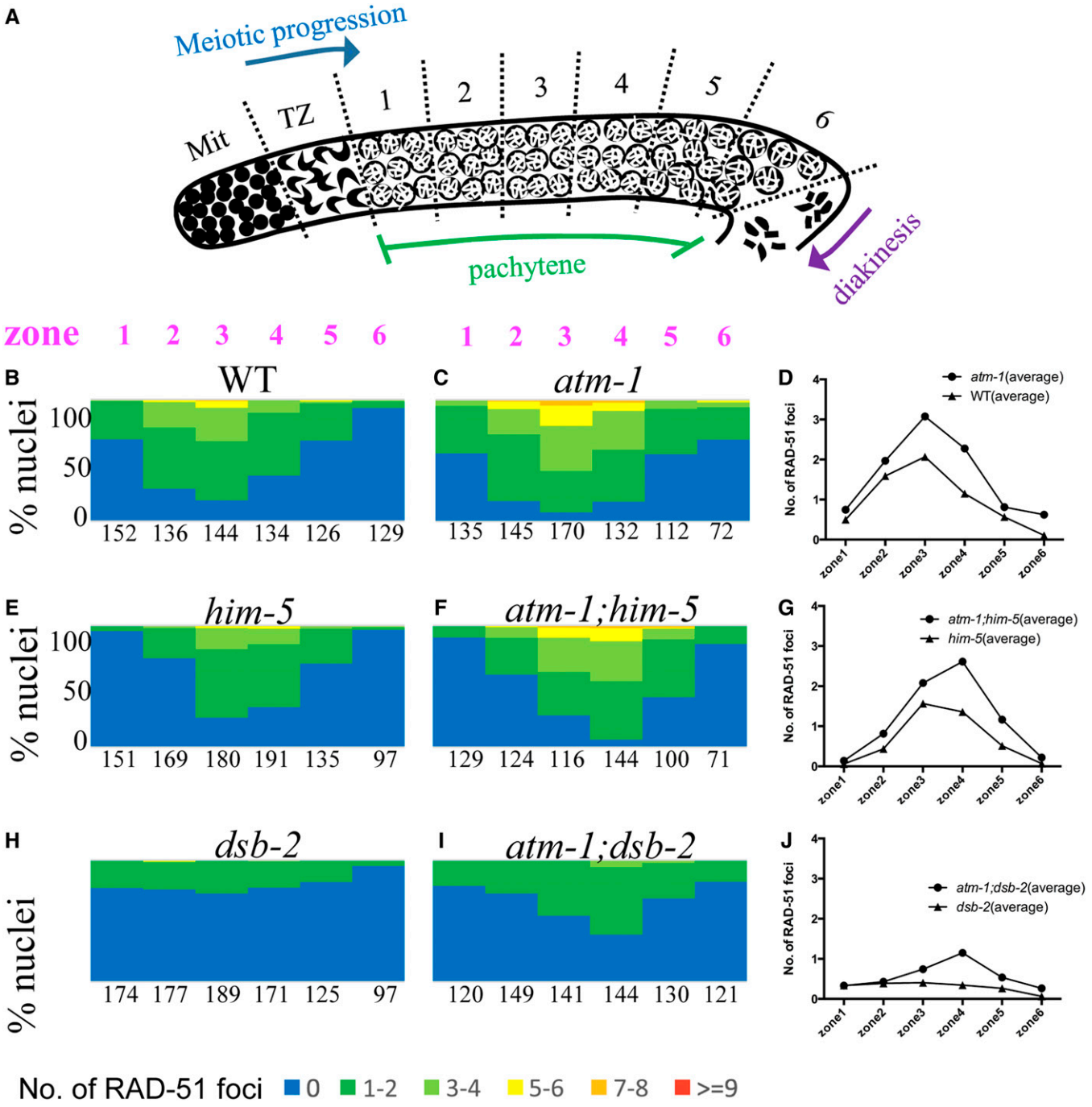

Figure 2 Early repair intermediates accumulate to a greater extent in *atm-1* mutants. (A) Schematic of the *C. elegans* germ line showing regions in which RAD-51 foci were quantified. Mit: Mitotic zone. TZ: transition zone. (B, C, E, F, H, and I) The percentage of nuclei in each zone containing the indicated number of RAD-51 foci shown in the color key at the bottom. Numbers represent total number of nuclei counted/zone for three gonads/genotype. (D, G, and J) Comparison of the average number of RAD-51 foci for each genotype. # = nuclei scored/3 germ lines/genotype. χ^{square}, *atm-1 vs.* N2; *atm-1;him-5 vs. him-5*; and *atm-1;dsb-2 vs. dsb-2*: $P < 0.0001$ for each. Representative images of germ lines are shown in Figure S1.

influence the timing, placement, and extent of DSB formation. ATM influences DSB formation in species as diverged as yeast and mice. In worms, *atm-1* mutant animals are homozygous viable and morphologically wild type, but variably have offspring with reduced viability and fecundity (Jones *et al.* 2012). In the germ line, an increased number of RAD-51 foci in *atm-1* mutant worms has been interpreted to support a widely conserved role in DSB formation (Checchi *et al.* 2014). In *C. elegans*, mutations in several of the SPO-11 accessory factors, including *him-5* and *dsb-2*, lead to a partial impairment in DSB formation, a subsequent decrease in RAD-51 foci, and a lack of COs on a subset of chromosomes (Meneely *et al.* 2012; Rosu *et al.* 2013). Since *atm-1* mutants have been shown to exhibit an excess of RAD-51 foci, which

Table 2 Early repair intermediates accumulate in *ATM-1* mutants

Genotype	No. of RAD-51 foci/nucleus
rad-54	31.08 ± 1.88
atm-1;rad-54	35.91 ± 1.64[a]
rad-54;him-5	22.83 ± 2.35
atm-1;rad-54;him-5	28.82 ± 3.73[b]

Analysis of late pachytene nuclei.
[a] *t* test, $P < 0.0001$.
[b] *t* test, $P < 0.0001$.

could reflect an excess of DSBs, we wanted to address how SPO-11 accessory factors and ATM-1 interact to impact CO formation. To test this, we constructed *atm-1;him-5* and *atm-1;dsb-2* double mutants and examined bivalent formation in single and double mutants by whole mount fixation and DAPI-staining.

The *atm-1;him-5* and *atm-1;dsb-2* double mutants contained significantly fewer bivalent chromosomes compared to *him-5* and *dsb-2* single mutants (Figure 1, A and B, $P < 0.01$). The six DAPI bodies observed in almost all wild-type germ cells correspond to the six bivalents formed between each pair of homologous chromosomes. In *him-5* and *dsb-2* single mutants, the number of DAPI bodies is increased since the nonexchange chromosomes separate from one another into discrete masses, or univalents (Figure 1, A and B and Meneely *et al.* 2012; Rosu *et al.* 2013). The *atm-1* single mutant showed ~5% of nuclei with fewer than six DAPI bodies (Figure 1, A and B). A subset of these may reflect whole chromosome fusions as the result of DNA repair defects (Jones *et al.* 2012). The formation of X:autosome fusions could explain the appearance of heritable, high frequency HIM (high incidence of males) lines in *atm-1* mutants (Jones *et al.* 2012). Surprisingly, close to 10% of *atm-1* mutant nuclei had seven DAPI bodies. The appearance of these DAPI-bodies was similar to *him-5*—with five well-formed bivalents and two uniformly sized univalents—which would explain the 2–3% HIM phenotype in the homozygous stocks. When *atm-1* mutations were combined with *him-5* or *dsb-2*, the percentage of univalent chromosomes was significantly increased. This was most striking in *atm-1;him-5* where >40% of diakinesis-stage nuclei contain more than eight DAPI bodies, the equivalent of two or more chromosomes with defective COs. Thus, while *atm-1* mutant animals have been reported to exhibit an increase in RAD-51 foci (Checchi *et al.* 2014), fewer COs appeared to form.

To validate these results, we also quantified COs using GFP::COSA-1—a fusion protein that localizes to the chiasma formed between homologs (Yokoo *et al.* 2012). Since worm chromosomes usually receive only a single CO, GFP::COSA-1 is seen as a single focus per homolog pair starting in mid- to late-pachytene. As reported previously, most *him-5* mutant nuclei have only five GFP::COSA-1 foci (Machovina *et al.* 2016), reflecting the loss of X chromosome CO formation (Figure 1C). Similarly, ~10% of nuclei in *atm-1* mutants contained only five GFP::COSA-1 foci, in accord with the fraction of diakinesis-stage nuclei that contain seven DAPI bodies in this mutant (Figure 1C). The number of GFP::COSA-1 foci was also significantly reduced in *atm-1;him-5* compared to *him-5* (Figure 1C, $P < 0.0001$). Together, these data implicate *atm-1* as a pro-CO factor in *C. elegans*.

We further tested the impact of *atm-1* loss on CO formation by examining recombination rates. We examined recombination rates in two large regions of chromosome III: the intervals between *dpy-18,unc-64*, which comprises >13 cM of the right arm of the chromosome, and between *dpy-1,lon-1* which spans ~14 cM from the middle of the left arm into the middle of the central gene cluster. In both intervals, no significant change in genetic distance was found in *atm-1* single mutants compared to wild type (Table 1). However, *atm-1;him-5* mutants gave a lower recombination rate compared to *him-5* mutants in both regions of chromosome III (Table 1). These data support the interpretation that *atm-1* mutations exacerbate the recombination defects caused by lack of *him-5* function. Together, these data strongly argue that COs are reduced in *atm-1;him-5* double mutants.

ATM-1 limits the number of early repair intermediates

To understand the nature of the increased RAD-51 foci in *atm-1* mutants (Checchi *et al.* 2014), but the decreased numbers of COs in *atm-1;him-5* and *atm-1;dsb-2* mutants, we considered the possibility that ATM-1 might have different roles in otherwise wild-type *vs.* CO-limiting situations. In this scenario, ATM-1 might limit DSBs under normal conditions (leading to the observed increase in RAD-51 foci), but, when confronted with subthreshold COs (COs on some chromosomes, but not all), it might function in a regulatory feedback loop to retain DSB activity (leading to reduced RAD-51 signals and fewer COs in the mutants). To determine if these different scenarios exist, we quantified RAD-51 foci in *atm-1* mutants. We note that prior studies showed a >95% concordance between RAD-51 foci and free ends marked by TUNEL staining, so that the former can be used as a surrogate to assess DSB levels (Mets and Meyer 2009). We first validated the results from prior studies (Checchi *et al.* 2014): using a different source of RAD-51 antibodies (see *Materials and Methods*), we also observed an increase in RAD-51 foci in *atm-1* mutant germ lines compared to wild type ($P < 0.0001$; Chi-square test; Figure 2, B–D and Figure S1, A and B). In *atm-1;him-5* and *atm-1;dsb-2* double mutants, distribution of RAD-51 foci in the pachytene germ line was altered compared to either single mutants ($P < 0.0001$; Chi-square test; Figure 2, D–I). Average RAD-51 levels were also elevated in *atm-1;him-5* compared to *him-5* ($P = 0.03$; Wilcoxon matched-pairs signed rank test, Figure 2F). These differences are particularly striking in light of our observations that COs were decreased in both *atm-1;him-5* and *atm-1;dsb-2* (Figure 1). Thus, we conclude that RAD-51 dynamics are affected by loss of *atm-1* function in wild type, and in mutants where COs are limiting.

RAD-51 accumulates on single-stranded, resected DNA ends as a filament that is dismantled upon stable strand exchange. Excessive RAD-51 signal would be seen if additional

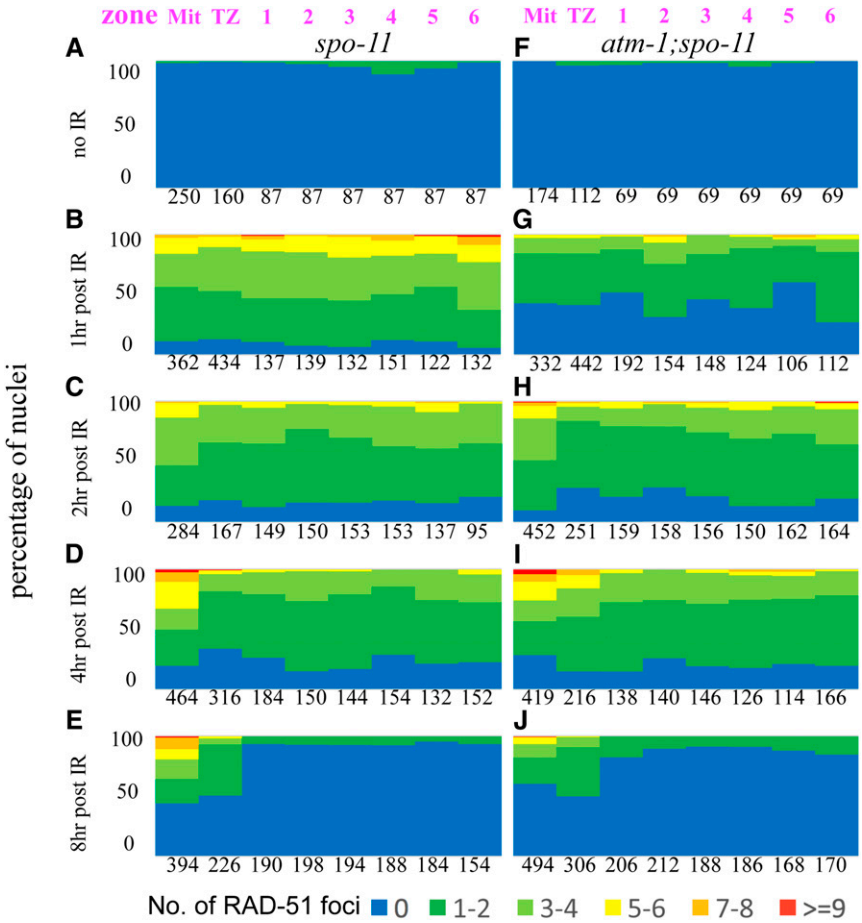

Figure 3 Loading of RAD-51 is delayed in *atm-1* mutants. For each region, the percentage of nuclei with a given number of RAD-51 foci is shown as a heat map from 0 to >9, as indicated below. Zones are shown in Figure 2A. # = nuclei scored/3 germ lines/genotype. (A–E) *spo-11* mutants. (F–J) *atm-1;spo-11* mutants. Shown in a time-course post-exposure to 10 Gy IR (A and F): unirradiated controls (B and G): 1 hr post-exposure shows reduced loading in *atm-1;spo-11*. (C and H): 2 hr and (D and I): 4 hr post-exposure loading is almost indistinguishable between control and *atm-1;spo-11*. (E and J): 8 hr post-exposure, most RAD-51 foci have been removed in the meiotic region of the germ line. We note that repair in the mitotic region is resolved with distinct kinetics.

DSBs were present or if the kinetics of RAD-51 filament formation or turnover were altered. To distinguish between these possibilities, we quantified RAD-51 foci in *rad-54* mutant animals in which strand invasion cannot occur, and, therefore, RAD-51 filaments accumulate. As expected, we observed increased RAD-51 foci in *atm-1 rad-54* single mutants compared to *rad-54* (Table 2 and Checchi *et al.* 2014). We also see more RAD-51 foci in *atm-1,rad-54;him-5* mutants compared to *rad-54;him-5* (Table 2). In both wild type and *him-5* mutants, loss of *atm-1* resulted in around five additional DSBs.

In addition to SPO-11-mediated DSBs, unrepaired mitotic or meiotic S phase DNA damage can contribute to pachytene accumulation of RAD-51. To determine if such damage is present in *atm-1* mutants, we analyzed RAD-51 foci in *spo-11* and *atm-1*; *spo-11* in which meiotic DSBs are not formed. If premeiotic (or meiotic S-phase) damage were carried through into pachytene, RAD-51 foci should be more prevalent in *atm-1;spo-11* compared to *spo-11*. We previously showed that ~10% of *spo-11* nuclei have GFP::COSA-1 foci and elicit CO feedback mechanisms (Machovina *et al.* 2016). This result was supported here by the appearance of a small number of RAD-51 foci in the pachytene region of *spo-11* mutants. By contrast, we saw very few RAD-51 foci in the premeiotic and meiotic regions *of atm-1;spo-11* (Figure 3, A and F and Figure S1, C and D). These results suggest that the extra RAD-51 foci in *atm-1* pachytene nuclei are not a consequence of premeiotic damage. Instead, these results point to a role for ATM-1 in limiting meiotic DSB formation and/or the early processing of these DSBs.

RAD-51 loading is impaired in atm-1 mutant animals

We next set out to determine if *atm-1* mutants might be defective in RAD-51 filament formation and/or processing. Since the appearance and disappearance of RAD-51 foci is influenced both by the extent of SPO-11 activity and the kinetics of RAD-51 loading and disassembly, it can be difficult to tease out the impact of altered DSB dynamics from altered behavior of RAD-51. To specifically examine the requirement for ATM-1 in RAD-51 loading, we therefore assayed RAD-51 focus formation in backgrounds where meiotic breaks are not made, comparing *atm-1;spo-11* with *spo-11* at various time points after exposure to IR. Surprisingly, at 1 hr post-IR, we observed many fewer RAD-51 foci in *atm-1;spo-11* double mutants compared to *spo-11* (Figure 3, B and G and Figure S1, E and F). These results intimate that early RAD-51 accumulation is impaired in *atm-1* mutants. At 2 hr post-IR, the number of RAD-51 foci in *atm-1;spo-11* reached levels comparable to *spo-11* 1-hr post-IR (Figure 2, C and H and Figure S1, G and H). RAD-51 foci in *atm-1;spo-11* and *spo-11* decreased comparably, as shown by the RAD-51 signals at 4 and 8 hr post-IR (Figure 2, D, E, I, and J). Thus, while RAD-51

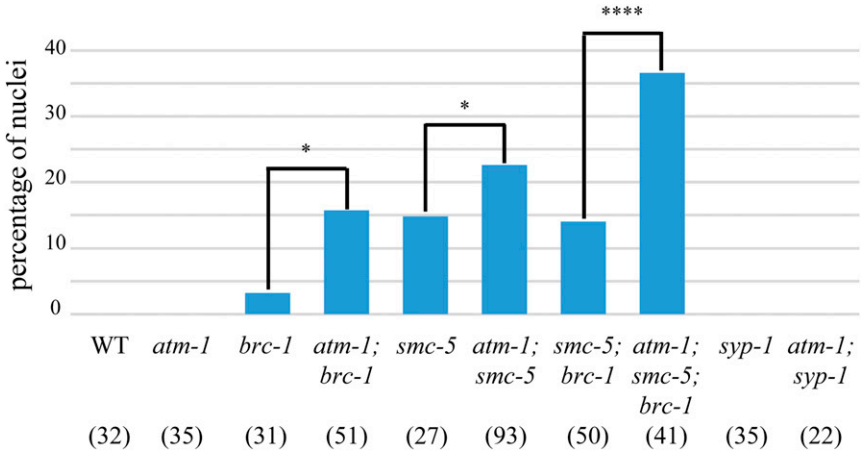

Figure 4 *atm-1* mutation increases fragmentation when intersister repair is impaired. Percentage of −1 nuclei containing DNA fragments as seen by DAPI staining. Numbers in brackets are the number of nuclei analyzed/genotype. $*P < 0.05$, $****P < 0.0001$ (χ^2 test).

focus formation may be affected by loss of *atm-1*, processing/removal of RAD-51 appears to be normal. While IR-induced and SPO-11 induced breaks are not treated identically in cells (Macaisne *et al.* 2018), these data raise the possibility that the excess RAD-51 foci seen in *atm-1*, *atm-1;him-5* and *atm-1;dsb-2* are not due to impaired RAD-51 processing, but rather most likely result from additional meiotic DSBs.

ATM-1 inhibits homolog-independent repair, channeling DSBs toward IH-HR

The bulk of meiotic DSBs are repaired through HR using either IH-HR or IS-HR repair pathways, and among these two pathways, only IH-HR can create chiasmata. We hypothesized that ATM-1 promotes CO formation by inhibiting processes that do not engage the homolog, thus channeling more DSBs going through IH-HR. Without this inhibition, DSBs would preferentially be repaired through IS-HR, or, as non-COs, leading to a deficit in COs. To test this hypothesis, we took advantage of two mutations that are known to impair homolog-independent repair: *brc-1* and *smc-5* (Adamo *et al.* 2008; Bickel *et al.* 2010). Mutants carrying either mutation had a small percentage of diakinesis-stage nuclei with chromosome fragments. In *syp* mutants, where synaptonemal complex (SC) formation is impaired, the homolog is not readily available for HR, and IS-HR is thought to be the major DSB repair pathway (Adamo *et al.* 2008; Bickel *et al.* 2010; Macaisne *et al.* 2018). In the *syp* mutant background, both *brc-1* and *smc-5* showed increased chromosome fragmentation. In contrast to *brc-1;syp-1* and *smc-5;syp-1*, we did not observe chromosome fragments in *atm-1;syp-1* mutants (Figure 4), indicating that all DSBs are repaired in this mutant context. By contrast, in *atm-1;brc-1* mutants, we found more nuclei with fragments compared to *brc-1* mutants (Figure 4, $P < 0.05$). A similar result was observed in *atm-1;smc-5* mutants, in which ~50% more nuclei contained DNA fragments compared to the *smc-5* single mutant. Further, *atm-1;smc-5;brc-1* triple mutants revealed substantially higher percentages of nuclei with fragments compared to *smc-5;brc-1* double mutants (Figure 4).

To determine if the increased number of chromosome fragments in the *atm-1* mutants arises simply as a result of excess meiotic DSBs formed in this background, we reasoned that *atm-1* should have no impact on the repair of DSBs induced by IR in the *smc-5;spo-11(−)* background. Consistent with our results in *spo-11*(+), more nuclei with fragments were observed in *atm-1;smc-5;spo-11* mutants compared to *smc-5;spo-11* after exposure to 10 Gy IR, while a similar percentage of nuclei with fragments was apparent in nonirradiated *smc-5;spo-11* and *atm-1;smc-5;spo-11* (Figure S2). Together, these data suggest that ATM-1 functions outside of DSB break formation to promote homolog-dependent repair.

ATM-1 functions on SPO-11 dependent and independent DSBs to promote CO formation when the number of DSBs is limiting

The CO defects in *atm-1;him-5* and *atm-1;dsb-2* appeared stronger than expected based on the mild CO defect in *atm-1* single mutants. This led us to investigate whether *atm-1* differentially affects DSB outcomes under low DSB *vs.* high DSB situations. We compared CO outcomes in *spo-11* and *atm-1;spo-11* mutants and after exposure to 2, 10, and 25 Gy IR (Machovina *et al.* 2016). Upon exposure to 2 or 10 Gy IR, nuclei of *atm-1;spo-11* double mutants exhibited greater numbers of DAPI bodies (fewer bivalents) at diakinesis compared to *spo-11* single mutants (Figure 5A and Figure S3). The impact on COs is not specific to the *spo-11* mutant background, as fewer bivalents were also seen in irradiated *atm-1;dsb-1* compared to *dsb-1* mutant animals that are also defective in meiotic DSB formation (Stamper *et al.* 2013) (Figure 5A and Figure S3). By contrast, no difference in CO outcomes was observed when *atm-1* and *atm-1;spo-11* mutants were exposed to 25 Gy IR, both mostly contained six DAPI bodies at diakinesis (Figure 5B). Since 1 Gy IR is expected to give around two meiotic DSBs (Machovina *et al.* 2016), and to increase linearly with dose, these results suggests that a threshold exists somewhere between 20 and 50 DSBs, beyond which *atm-1* dysfunction in DSB repair is overcome.

Our analysis of *atm-1;him-5* mutants provided support for a threshold of DSBs for ATM-1 regulation. As discussed above, in *atm-1;him*-5 double mutants, DSBs appeared to be shunted into non-CO repair pathways. However, the

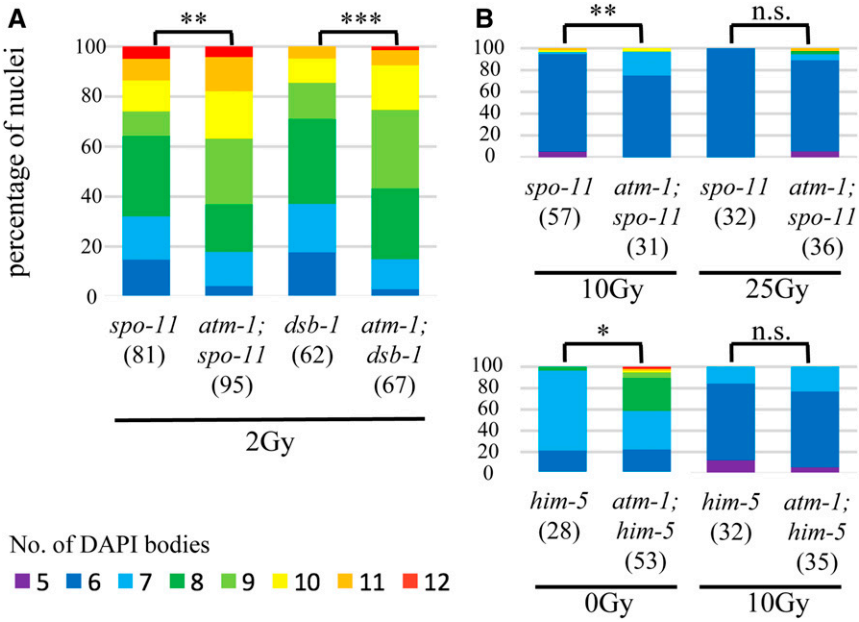

Figure 5 *atm-1* acts on exogenous DSBs as well as SPO-11 induced DSBS to promote COs within a threshold of total DSBs. Quantification of DAPI bodies in −1 nuclei for different doses of IR. Color key below. (A) 2 Gy IR leads to more COs in *atm-1;spo-11* and *atm-1;dsb-1* compared to control *spo-11 dsb-1*, respectively. (B) *atm-1* loss is overpowered by high numbers of DSBs, between 10 and 25 Gy (20–50 DSBs) in *atm-1*; *spo-11* (top); below 10 Gy (20 additional breaks) in *atm-1;him-5* (∼28 endogenous breaks). $*P < 0.05$, $**P < 0.01$, $***P < 0.001$, n.s. = no significant difference, two-tailed Mann Whitney test.

addition of 10 Gy IR in this genetic background was sufficient to drive DSBs into the IH-HR pathways, leading to six bivalents in most diakinesis nuclei (Figure 5B). The exposure of *atm-1;him-5* to 10 Gy IR would induce ∼20 more DSBs, bringing break levels to near those in *atm-1;spo-11* + 25 Gy. Together, these results support a role for ATM-1 in repair pathway choice when the number of DSBs is under a threshold of ∼30–50 DSBs. When above this threshold, ATM-1 function appears to be bypassed.

ATL-1 contributes to CO formation by influencing accumulation of early break intermediates

One candidate for subsuming ATM functions is ATR—the other major kinase involved in the DNA damage response. ATR is encoded by *atl-1* (ATM-Like) and is an essential gene that is required for mitotic DNA repair (Garcia-Muse and Boulton 2005; reviewed in Budzowska and Kanaar 2009). Loss of *atl-1* leads to both macronuclei and micronuclei due to the impairment in DNA damage signaling (Figure S4A). In nuclei that go on to make oocytes, we observed nearly 25% with only five DAPI bodies (Figure 6A), presumably reflecting the formation of chromosome fusions in response to DNA damage. Another 5% of nuclei had more than six DAPI bodies (Figure 6A), suggesting that, like *atm-1*, *atl-1* is required for a full complement of CO exchanges. In *dsb-2* and *him-5* mutants, lack of ATL-1 function also reduced CO numbers (Figure 6A). Thus, we conclude that ATL-1, like ATM-1, contributes to CO formation when DSBs are limiting.

To determine if ATL-1 directly impacts DSBs/early repair processing, we analyzed RAD-51 dynamics. Two aspects of RAD-51 accumulation distinguished *atl-1* mutants from wild type. First, the appearance of RAD-51 signals differed: a subset of *atl-1* mutant nuclei exhibited very high RAD-51 signals (Figure 7, A–C). Since the RAD-51 signal was so extensive in some nuclei, we quantified these images by binning the nuclei based on number of foci that were observed (Figure 7, H–J). The second distinct aspect of *atl-1* mutants was the timing of RAD-51 focus formation: in *atl-1*, RAD-51 foci were observed in most nuclei from the TZ through the pachytene–diplotene border in *atl-1* (Figure 7, C and H); whereas, in wild type, foci only started to accumulate in the TZ, and were seen in most nuclei only at midpachytene (Figure 2B, Figure 7, B and H, and Figure S1A).

The differences in RAD-51 accumulation, together with the known role for *atl-1* in mitotic cell divisions (Abraham 2001; Garcia-Muse and Boulton 2005; Lawrence *et al.* 2015), led us to explore whether any of RAD-51 foci could be explained by an increase in carry-through damage from mitotic divisions. In *spo-11;atl-1*, there was substantial RAD-51 signal in the pachytene region, indicating the presence DNA damage that arose independently from meiotic-induced DSBs (Figure 7D; cf. *spo-11* in Figure S1C). We note that this damage can contribute to CO formation as we saw an increase in bivalents in *spo-11;atl-1* diakinesis-stage oocytes (Figure 6B). Irradiation of *spo-11;atl-1* mutants with 10 Gy IR showed efficient RAD-51 loading within 1 hr post-IR, and, as in the *atl-1* background, a subset of the signal appeared in stretches (as opposed to smaller foci; Figure S4D). Since these stretches were not seen in the irradiated *spo-11* mutant germ lines (Figure S1, E and G), we infer that these stretches do not result from two adjacent DSBs, but rather from a defect that is specific to the *atl-1* mutant. Similar stretches of RAD-51 have been seen in meiotic mutants with defects in RAD-51 filament maturation (Mets and Meyer 2009; Ward *et al.* 2010), raising the possibility that ATL-1 limits/antagonizes RAD-51 loading. *atl-1* loss would therefore lead to excessive, and perhaps untimely, RAD-51 filament formation.

We also observed RAD-51 foci in the TZ of *atl-1,him-5* double-mutant animals (Figure 7, A and E). In this mutant background, the kinetics of RAD-51 formation and loss are similar to *atl-1* single mutants, appearing earlier and brighter

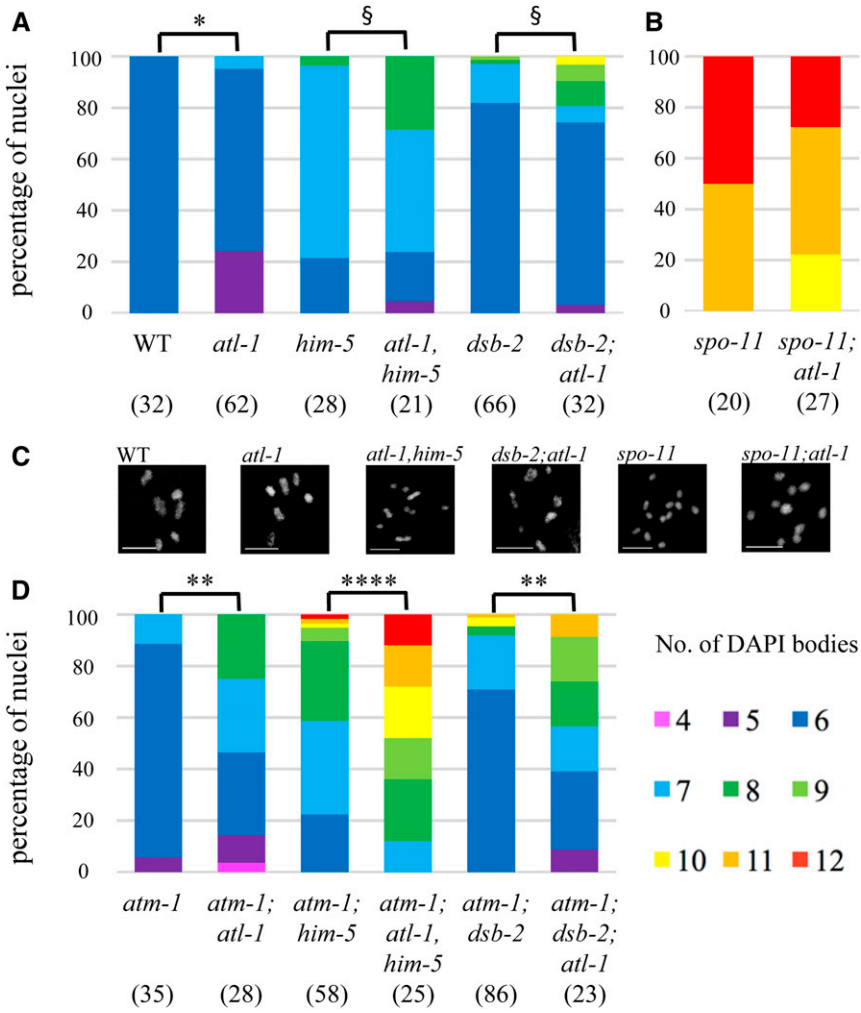

Figure 6 *atl-1* mutant animals exhibit defects in CO formation in wild-type and DSB-limiting situations. (A, B, and D). Quantification of DAPI bodies in −1 nuclei containing the indicated number of DAPI bodies. $*P < 0.05$, $**P < 0.01$, $****P < 0.0001$, two-tailed Mann-Whitney test. $^{§}P < 0.05$, Fisher's exact test. (A) *atl-1* has an increase in univalents alone or in combination with *him-5* and *dsb-2*. (B) *atl-1* mutants increase bivalents in *spo-11*, indicating a substantial amount of carry-though DNA damage from the mitosis and meiotic S phase. (C) Representative diakinesis-stage nuclei of different genotypes showing normal karyotype (wt) and mutant background with different proportions of bivalents and univalents. (D) Quantification of DAPI bodies in *atm-1;atl-1* double mutants alone or with DSB-defective mutations shows synergistic effects from the loss of both gene functions.

that in wild type (Figure 7H). However, the number of nuclei with RAD-51 staining was reduced in *atl-1,him-5* compared to *atl-1* mutants, as expected since *him-5* mutations partially impair DSB formation. The number of RAD-51-positive nuclei was also reduced compared to *him-5* (Figure 7, E, F, H, and I), whereas upwards of 70% of *him*-5 mutant nuclei stained weakly for RAD-51 at its peak, <30% of *atl-1,him*-5 nuclei showed RAD-51 foci (Figure 7, H and I). Of those that had foci, a subset had the very strong RAD-51 signals that were associated with carry-through damage, described above. Thus, 30% is an overrepresentation of the number of nuclei with *bona fide* meiotic damage. These data show that *atl-1* and *him-5* both contribute to RAD-51-focus formation, and that *atl-1* is epistatic to *him-5* for timing of RAD-51 formation.

In yeast and mice, ATM and ATR function together to establish DSB homeostasis (Carballo *et al.* 2013), with ATM inhibiting DSBs to prevent over-accumulation and ATR promoting DSBs to ensure sufficient COs can be made. We therefore wanted to know what the impact on meiotic CO formation would be when both *atm-1* and *atl-1* are mutated. To our surprise, *atm-1;atl-1* mutants showed a severe defect in CO formation: whereas both *atm-1* and *atl-1* single mutants exhibited mild CO defects (Figure 6, A and C). In the double mutants, >70% of nuclei had CO defects, of which >50% contain one or more pairs of univalents. Loss of both *atm-1* and *atl-1* also exacerbated the CO defect associated with *him-5* and *dsb*-2 (Figure 6C). Thus, despite seemingly antagonistic roles on RAD-51 formation, *atm-1;atl-1* double mutants are significantly impaired in CO formation.

Consistent with these results, we saw very few RAD-51 foci in early and midpachytene nuclei in *atm-1;atl-1* (Figure 7, G, H, and J). At late pachytene, almost all nuclei stained strongly for RAD-51, a phenotype seen in neither of the single mutants. It is unlikely that all of these nuclei are destined for apoptosis since we observed diakinesis-stage oocytes with well-formed bivalents (Figure 6C). Instead, this data suggests a change in CO regulation in the double mutant (discussed below).

CO feedback is impacted by loss of atm-1 and atl-1

Defects in CO formation are thought to activate surveillance systems that feed back onto the break machinery to maintain DSB competency when COs are not detected (Rosu *et al.* 2013; Stamper *et al.* 2013; Machovina *et al.* 2016; Nadarajan *et al.* 2017; Pattabiraman *et al.* 2017). The activity of this feedback mechanism is spatially observed in the pachytene germ line

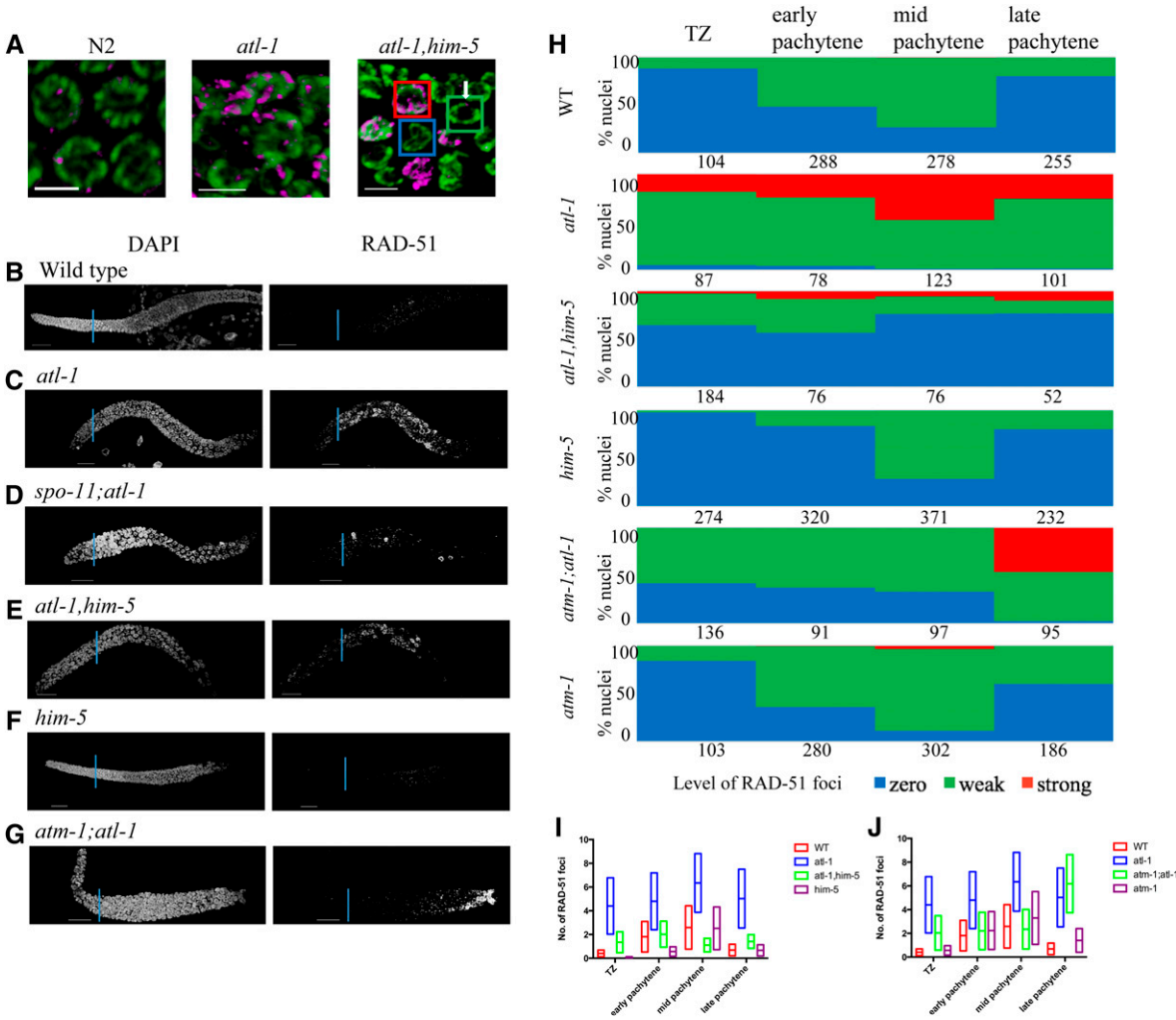

Figure 7 RAD-51 loading is altered by *atl-1*. (A) RAD-51 staining in pachytene nuclei of wild type N2, *atl*-1, and *atl-1 him*-5. RAD-51 (magenta); DAPI (green). Bar, 5 μm. The squares represent the three class of nuclei quantified in (C): Zero RAD-51 foci (blue); Weak staining (green); strong staining (red). (B–G) Representative images of DAPI and RAD-51 stained gonads from 1-day-old adults of indicated genotype. (H) Proportions of nuclei containing 0 (blue), 1–6 (green, weak), or >6 foci (red, strong) RAD-51 foci in the leptotene-pachytene regions of the germ line as described in *Materials and Methods*. Numbers indicate total number of nuclei counted for each region for at least three germ lines/genotype. (I and J) Range and average of RAD-51 foci for germ lines quantified in (H) for shown genotypes.

as an extended region of DSB-1 and DSB-2 staining in CO-deficient worms (Rosu *et al.* 2013; Stamper *et al.* 2013). We reasoned that the increased number of RAD-51 foci observed in *atm-1* mutants might be explained by changes in DSB-2 regulation. We observed that DSB-2 staining in *atm-1* mutants was shifted proximally—turning on slightly later than in wild type relative to the onset of leptotene (Figure 8). It also persisted slightly longer, taking, on average, ~7% more of the pachytene region than wild type (Figure 8). The small number of excess DSBs in *atm-1* may be attributed to this increased window of opportunity for DSB-2- (and by inference, DSB-1-) dependent breaks. We also observed that *atm-1* activity was not required to induce (or maintain) the extended domain of DSB-2 in *him-5* mutants (Figure 8). Thus, we posit that the reduction in COs in *atm-1;him-5* cannot be explained by inhibition of DSB-2.

In *atl-1* mutants, DSB-2 staining spanned only ~33% of the leptotene to pachytene region, whereas it comprised ~45% in wild type (Figure 8). This result suggests that the CO-dependent deactivation of DSB-2 occurred more rapidly in *atl-1* mutants. *him-5* is epistatic to *atl-1*, as was seen by the slight delay in DSB-2 onset, and much extended domain of staining in *atl-1,him-5* double mutants. These phenotypes are best explained by the role of role HIM-5 in promoting DSB formation, *i.e.*, delaying the formation of DSBs and preventing DSBs on the X chromosome (Meneely *et al.* 2012).

In the *atm-1;atl-1* mutants, the DSB-2 region was distinct from either single mutant: DSB-2 was activated as in wild type, yet it persisted until very late pachytene. The extension of DSB-2 staining was similar to that seen in *him-5* mutants, suggesting it may also reflect the diminished COs that form in the double mutants.

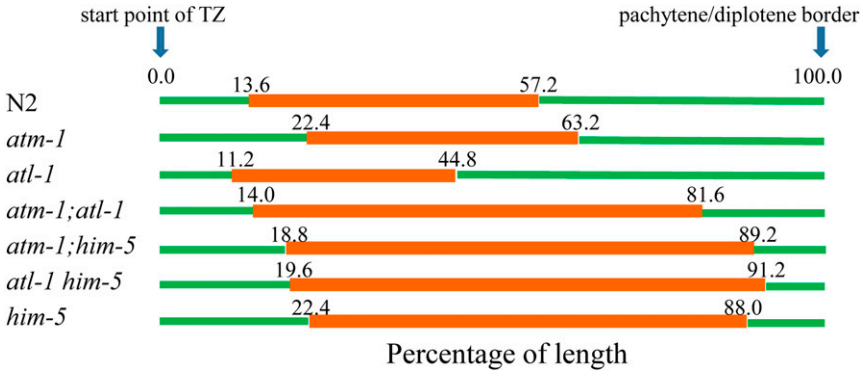

Figure 8 DSB-2 staining manifests different kinetics in the absence of ATM-1 or ATL-1 functions. Proportion of length of the germline region from meiotic onset to the pachytene/diplotene border that stain positive for nuclear localized DSB-2. Non-stained regions (green); stained (red). Genotypes are shown to the left with the average DSB-2 region depicted in orange (n = 3, 6, 7, 4, 4, 5, 6 for N2, *atm-1*, *atl-1*, *atm-1;atl-1*, *atm-1;him-5*, *atl-1 him-5*, and *him-5*, respectively).

Discussion

ATM-1 and ATL-1 have both unique and overlapping functions in worm meiosis that influence the formation of COs. We have shown that these genes have antagonistic and synergistic roles in DSB and CO formation, as summarized in our proposed model in Figure 9. We posit that, upon SPO-11 activation, a small number of initial DSBs (<10) are formed, which is sufficient to activate ATM-1 and ATL-1. Both proteins would then influence the activation of DSB-2 (perhaps through DSB-1): ATL-1 directly and ATM-1 through the regulation of early events post-DSB formation, perhaps resection. The lack of input from ATL-1 would explain the reduction in DSBs seen in *atl-1* mutants. Delayed resection could explain the delayed activation of the DSB-2 feedback loop and its prolonged localization in *atm-1* mutants. We propose that ATM-1 and ATL-1 then influence the transition from resection to an IH-CO competent RAD-51 filament. In the case of ATM-1, our *atm-1;spo-11 + IR* data predict a role in the timely recruitment of RAD-51. This delay could be a consequence of its role in resection or its role in influencing RAD-51 loading. Further studies will be required to determine if ATM-1 has the same impact on RAD-51 recruitment at SPO-11-induced breaks.

To our surprise, we found that, despite increased RAD-51 foci, COs are diminished in *atm-1* mutants. This reduction could be due to the ability of ATM-1 to influence the timely recruitment of RAD-51 (assuming SPO-11 induced breaks are treated the same at IR-induced breaks) and/or to shunt meiotic DSBs into the IH-CO repair pathway. In its absence, non-CO repair pathways are favored. Thus, *atm-1* appears to function antagonistically on different aspects of CO formation, limiting the total number of DSBs, but increasing the likelihood that DSBs are repaired by IH-CO repair. ATL-1 also appears to have an antagonistic function with decreased numbers of DSBs; yet, excessive RAD-51 loading seen in the *atl-1* mutant animals. These mutually antagonistic behaviors can be explained by negative and positive feedback loops and built-in functional redundancy (Figure 9) that illustrate the extensive and precise machinations required to ensure that COs occur on each chromosome.

Our model posits that, as in other systems (reviewed in Moriel-Carretero *et al.* 2018), DSBs activate ATM-1 to promote timely resection and subsequent activation of ATL-1. Resected ends and ATL-1 would both promote a secondary wave of DSBs that are induced through activation of DSB-2, and by inference DSB-1 (Stamper *et al.* 2013). This explains the decreased RAD-51 foci in *atl-1* mutants and the delay in DSB-2 loading in *atm-1* mutants. The increased number of RAD-51 foci in *atm-1* mutants might suggest that ATM-1 negatively regulates DSB formation. Alternatively, the five to six extra DSBs (Table 2) that are made could also be explained by persistent activation of the CO surveillance system (Machovina *et al.* 2016; Figure 9). In this case, a bias for IS-HR or non-COs in *atm-1* mutants would result in later CO formation and tardy deactivation of DSB-1/2. ATL-1 (and perhaps ATM-1) are likely to be regulating DSBs and DSB-2 localization through phosphorylation of SPO-11 and/or one or more its accessory factors. Bioinformatic analysis identified potential (S/T)Q sites in all 10 factors known to influence DSB formation, supporting the possibility that one or more are direct targets of ATL-1 (or ATM-1) (Figure S5). Our analyses of *atm-1;dsb-2* and *atm-1;him-5* double mutants showed increased DSBs (seen as RAD-51 foci), ruling out DSB-2 and HIM-5 as the sole targets of ATM/ATR signaling, although they may have redundant functions. Further studies are needed to identify relevant targets in the DSB machinery.

Our observation that RAD-51 loading is delayed in *atm-1* mutants post-IR suggests that ATM-1 facilitates efficient formation of the RAD-51 filament. In mitosis, both ATM and ATR activate resection activities with ATR functioning as well to attenuate Exo1-mediated activities (reviewed in Gobbini *et al.* 2013). In meiosis, recent studies have shown that yeast ATM1/Tel1 promotes resection of early DSBs (Joshi *et al.* 2015) and that mouse ATM helps to initiate and promote resection (Mimitou *et al.* 2017). A defect in resection could explain the delay in RAD-51 recruitment in *atm-1;spo-11* post-IR. A likely downstream target to regulate resection and RAD-51 loading (serving as protein X in Figure 9) is RAD-50, whose homologs are targets of ATM signaling in other systems (Gatei *et al.* 2011). In worms, RAD-51 loading in the early- to midpachytene region requires RAD-50 activity, whereas late pachytene loading is RAD-50-independent (Hayashi *et al.* 2007). The transition between these two states is thought to correspond to the switch from IH-HR to IS-HR. By promoting RAD-50 activity, ATM-1 could therefore

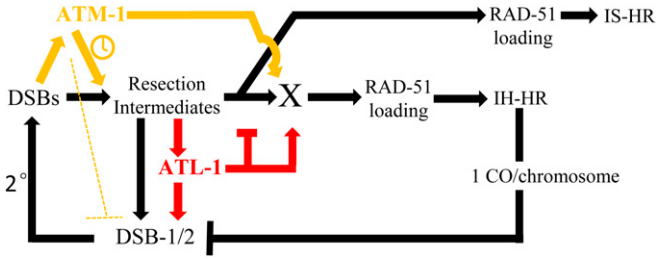

Figure 9 Model for ATM-1 and ATL-1 functions during meiosis. We propose that ATM-1 is activated by DSBs and then promotes the timely resection of ends and repair using the homolog as a repair template. The excess RAD-51 foci in *atm-1* mutants could be explained if ATM-1 inhibits DSBs (dotted line), perhaps through DSB-1, but possibly SPO-11 or other accessory factors. Alternatively, delayed resection and IH-CO formation could keep the feed-forward loop active longer to allow additional DSBs to be made. We further posit that ATL-1 is activated by resection intermediates, and both ATL-1 and a subset of pre-RAD-51 repair intermediates feed forward to promote additional DSB formation. ATL-1 then inhibits extensive resection and redundantly to ATM-1 helps to promote RAD-51 loading. These two activities can explain the delayed, excessive RAD-51 loading in *atm-1;atl-1* double mutants.

assure the repair of meiotic DSBs by IH-HR; in its absence, RAD-50 activity would be attenuated, and IS-HR/non-CO repair would be favored.

ATR has also been implicated in resection control, both promoting and restraining extensive EXO1 activity (Tomimatsu *et al.* 2017). Our observation that a subset of ATR mutants present with large RAD-51 aggregates intimates that the latter function, at least, of ATR may be conserved in worm ATL-1. The rapid disappearance of nuclear localized DSB-2 in *atl-1* mutants could be explained by the formation of longer resected ends that would be converted more rapidly into IH-COs, leading to cessation of DSB formation by CO feedback (Machovina *et al.* 2016). Together with our analysis of ATM-1, these data raise the intriguing possibility that different resection tract lengths could influence the CO *vs.* non-CO decision.

Based on their mutually antagonistic behavior on DSBs/RAD-51 foci formation, we explored the impact of loss of both ATM-1 and ATL-1 functions. In *atm-1;atl-1* double mutants, both RAD-51 foci and COs are decreased (Figure 6C and Figure S4D). This suggests that *atl-1* has an additional role in promoting RAD-51 loading that is redundant with ATM-1. Although depicted as a shared target gene, this may reflect one or more downstream roles. We envision that, in the double mutant background, the DSB feedback loop is activated via resected ends (through DSB-1 or other accessory factors), the ends are hyper-resected due to loss of *atl-1*, but RAD-51 loading is significantly delayed due to the joint functions of ATL-1 and ATM-1 on RAD-51 loading, which are relieved when the block to IS-HR is relaxed in late pachytene, leading to the excessive loading of RAD-51 in the *atm-1;atl-1* double mutant.

These data reveal the complex interplay between ATM and ATR signaling in meiosis that ultimately helps determine both the number of DSBs and the formation of IH-COs. These studies highlight multiple potential targets of ATM-1 and ATL-1 and provide the basis for the future identification and analysis of specific substrates. These studies also illuminate the evolutionary conserved of antagonism between ATM and ATR that is necessitated by the requirement for CO formation on each chromosome.

Acknowledgments

The authors thank Kara Bernstein, Arjumand Ghazi, Arthur Levine, Nicolas Macaisne, Brooke McClendon, and Logan Russell for critical reading of the manuscript. Gratitude is extended to Sarit Smolikove for sharing her anti-RAD-51 antibody. Some strains were provided by the CGC, which is funded by the National Institutes of Health (NIH) Office of Research Infrastructure Programs (P40 OD010440). W.L. was funded by Tsinghua University School of Medicine; J.Y. was funded by Pennsylvania Formula Funds and National Institute of General Medical Sciences (NIGMS)/NIH (GM104007).

Literature Cited

Abraham, R. T., 2001 Cell cycle checkpoint signaling through the ATM and ATR kinases. Genes Dev. 15: 2177–2196. https://doi.org/10.1101/gad.914401

Adamo, A., P. Montemauri, N. Silva, J. D. Ward, S. J. Boulton *et al.*, 2008 BRC-1 acts in the inter-sister pathway of meiotic double-strand break repair. EMBO Rep. 9: 287–292. https://doi.org/10.1038/sj.embor.7401167

Anderson, C. M., A. Oke, P. Yam, T. Zhuge, and J. C. Fung, 2015 Reduced crossover interference and increased ZMM-independent recombination in the absence of Tel1/ATM. PLoS Genet. 11: e1005478. https://doi.org/10.1371/journal.pgen.1005478

Barlow, C., S. Hirotsune, R. Paylor, M. Liyanage, M. Eckhaus *et al.*, 1996 Atm-deficient mice: a paradigm of ataxia telangiectasia. Cell 86: 159–171. https://doi.org/10.1016/S0092-8674(00)80086-0

Barlow, C., M. Liyanage, P. B. Moens, M. Tarsounas, K. Nagashima *et al.*, 1998 Atm deficiency results in severe meiotic disruption as early as leptonema of prophase I. Development 125: 4007–4017.

Bickel, J. S., L. Chen, J. Hayward, S. L. Yeap, A. E. Alkers *et al.*, 2010 Structural maintenance of chromosomes (SMC) proteins promote homolog-independent recombination repair in meiosis crucial for germ cell genomic stability. PLoS Genet. 6: e1001028. https://doi.org/10.1371/journal.pgen.1001028

Brenner, S., 1974 The genetics of Caenorhabditis elegans. Genetics 77: 71–94.

Budzowska, M., and R. Kanaar, 2009 Mechanisms of dealing with DNA damage-induced replication problems. Cell Biochem. Biophys. 53: 17–31. https://doi.org/10.1007/s12013-008-9039-y

Carballo, J. A., S. Panizza, M. E. Serrentino, A. L. Johnson, M. Geymonat *et al.*, 2013 Budding yeast ATM/ATR control meiotic double-strand break (DSB) levels by down-regulating Rec114, an essential component of the DSB-machinery. PLoS Genet. 9: e1003545. https://doi.org/10.1371/journal.pgen.1003545

Checchi, P. M., K. S. Lawrence, M. V. Van, B. J. Larson, and J. Engebrecht, 2014 Pseudosynapsis and decreased stringency of meiotic repair pathway choice on the hemizygous sex

chromosome of Caenorhabditis elegans males. Genetics 197: 543–560. https://doi.org/10.1534/genetics.114.164152

Cooper, T. J., K. Wardell, V. Garcia, and M. J. Neale, 2014 Homeostatic regulation of meiotic DSB formation by ATM/ATR. Exp. Cell Res. 329: 124–131. https://doi.org/10.1016/j.yexcr.2014.07.016

Garcia, V., S. Gray, R. M. Allison, T. J. Cooper, and M. J. Neale, 2015 Tel1(ATM)-mediated interference suppresses clustered meiotic double-strand-break formation. Nature 520: 114–118. https://doi.org/10.1038/nature13993

Garcia-Muse, T., and S. J. Boulton, 2005 Distinct modes of ATR activation after replication stress and DNA double-strand breaks in Caenorhabditis elegans. EMBO J. 24: 4345–4355. https://doi.org/10.1038/sj.emboj.7600896

Gatei, M., B. Jakob, P. Chen, A. W. Kijas, O. J. Becherel *et al.*, 2011 ATM protein-dependent phosphorylation of Rad50 protein regulates DNA repair and cell cycle control. J. Biol. Chem. 286: 31542–31556. https://doi.org/10.1074/jbc.M111.258152

Gobbini, E., D. Cesena, A. Galbiati, A. Lockhart, and M. P. Longhese, 2013 Interplays between ATM/Tel1 and ATR/Mec1 in sensing and signaling DNA double-strand breaks. DNA Repair (Amst.) 12: 791–799. https://doi.org/10.1016/j.dnarep.2013.07.009

Gray, S., R. M. Allison, V. Garcia, A. S. Goldman, and M. J. Neale, 2013 Positive regulation of meiotic DNA double-strand break formation by activation of the DNA damage checkpoint kinase Mec1(ATR). Open Biol. 3: 130019. https://doi.org/10.1098/rsob.130019

Hayashi, M., G. M. Chin, and A. M. Villeneuve, 2007 C. elegans germ cells switch between distinct modes of double-strand break repair during meiotic prophase progression. PLoS Genet. 3: e191. https://doi.org/10.1371/journal.pgen.0030191

Jones, M. R., J. C. Huang, S. Y. Chua, D. L. Baillie, and A. M. Rose, 2012 The atm-1 gene is required for genome stability in Caenorhabditis elegans. Mol. Genet. Genomics 287: 325–335. https://doi.org/10.1007/s00438-012-0681-0

Joshi, N., M. S. Brown, D. K. Bishop, and G. V. Borner, 2015 Gradual implementation of the meiotic recombination program via checkpoint pathways controlled by global DSB levels. Mol. Cell 57: 797–811. https://doi.org/10.1016/j.molcel.2014.12.027

Joyce, E. F., M. Pedersen, S. Tiong, S. K. White-Brown, A. Paul *et al.*, 2011 Drosophila ATM and ATR have distinct activities in the regulation of meiotic DNA damage and repair. J. Cell Biol. 195: 359–367. https://doi.org/10.1083/jcb.201104121

Lange, J., J. Pan, F. Cole, M. P. Thelen, M. Jasin *et al.*, 2011 ATM controls meiotic double-strand-break formation. Nature 479: 237–240. https://doi.org/10.1038/nature10508

Lawrence, K. S., T. Chau, and J. Engebrecht, 2015 DNA damage response and spindle assembly checkpoint function throughout the cell cycle to ensure genomic integrity. PLoS Genet. 11: e1005150. https://doi.org/10.1371/journal.pgen.1005150

Macaisne, N., Z. Kessler, and J. L. Yanowitz, 2018 Meiotic double-strand break proteins influence repair pathway utilization. Genetics 210: 843–856. https://doi.org/10.1534/genetics.118.301402

Machovina, T. S., R. Mainpal, A. Daryabeigi, O. McGovern, D. Paouneskou *et al.*, 2016 A surveillance system ensures crossover formation in C. elegans. Curr. Biol. 26: 2873–2884. https://doi.org/10.1016/j.cub.2016.09.007

MacQueen, A. J., and A. Hochwagen, 2011 Checkpoint mechanisms: the puppet masters of meiotic prophase. Trends Cell Biol. 21: 393–400. https://doi.org/10.1016/j.tcb.2011.03.004

Martini, E., R. L. Diaz, N. Hunter, and S. Keeney, 2006 Crossover homeostasis in yeast meiosis. Cell 126: 285–295. https://doi.org/10.1016/j.cell.2006.05.044

McClendon, T. B., R. Mainpal, F. R. Amrit, M. W. Krause, A. Ghazi *et al.*, 2016 X chromosome crossover formation and genome stability in Caenorhabditis elegans are independently regulated by xnd-1. G3 (Bethesda) 6: 3913–3925. https://doi.org/10.1534/g3.116.035725

Meneely, P. M., O. L. McGovern, F. I. Heinis, and J. L. Yanowitz, 2012 Crossover distribution and frequency are regulated by him-5 in Caenorhabditis elegans. Genetics 190: 1251–1266. https://doi.org/10.1534/genetics.111.137463

Mets, D. G., and B. J. Meyer, 2009 Condensins regulate meiotic DNA break distribution, thus crossover frequency, by controlling chromosome structure. Cell 139: 73–86. https://doi.org/10.1016/j.cell.2009.07.035

Mimitou, E. P., S. Yamada, and S. Keeney, 2017 A global view of meiotic double-strand break end resection. Science 355: 40–45. https://doi.org/10.1126/science.aak9704

Moriel-Carretero, M., P. Pasero, and B. Pardo, 2018 DDR Inc., one business, two associates. Curr. Genet. 65: 445–451. .https://doi.org/10.1007/s00294-018-0908-7

Nadarajan, S., T. J. Lambert, E. Altendorfer, J. Gao, M. D. Blower *et al.*, 2017 Polo-like kinase-dependent phosphorylation of the synaptonemal complex protein SYP-4 regulates double-strand break formation through a negative feedback loop. eLife 6: e23437. .https://doi.org/10.7554/eLife.23437

Pattabiraman, D., B. Roelens, A. Woglar, and A. M. Villeneuve, 2017 Meiotic recombination modulates the structure and dynamics of the synaptonemal complex during C. elegans meiosis. PLoS Genet. 13: e1006670. https://doi.org/10.1371/journal.pgen.1006670

Rosu, S., K. A. Zawadzki, E. L. Stamper, D. E. Libuda, A. L. Reese *et al.*, 2013 The C. elegans DSB-2 protein reveals a regulatory network that controls competence for meiotic DSB formation and promotes crossover assurance. PLoS Genet. 9: e1003674. https://doi.org/10.1371/journal.pgen.1003674

Stamper, E. L., S. E. Rodenbusch, S. Rosu, J. Ahringer, A. M. Villeneuve *et al.*, 2013 Identification of DSB-1, a protein required for initiation of meiotic recombination in Caenorhabditis elegans, illuminates a crossover assurance checkpoint. PLoS Genet. 9: e1003679. https://doi.org/10.1371/journal.pgen.1003679

Tomimatsu, N., B. Mukherjee, J. L. Harris, F. L. Boffo, M. C. Hardebeck *et al.*, 2017 DNA-damage-induced degradation of EXO1 exonuclease limits DNA end resection to ensure accurate DNA repair. J. Biol. Chem. 292: 10779–10790. https://doi.org/10.1074/jbc.M116.772475

Ward, J. D., D. M. Muzzini, M. I. Petalcorin, E. Martinez-Perez, J. S. Martin *et al.*, 2010 Overlapping mechanisms promote postsynaptic RAD-51 filament disassembly during meiotic double-strand break repair. Mol. Cell 37: 259–272. https://doi.org/10.1016/j.molcel.2009.12.026

Xu, Y., T. Ashley, E. E. Brainerd, R. T. Bronson, M. S. Meyn *et al.*, 1996 Targeted disruption of ATM leads to growth retardation, chromosomal fragmentation during meiosis, immune defects, and thymic lymphoma. Genes Dev. 10: 2411–2422. https://doi.org/10.1101/gad.10.19.2411

Yokoo, R., K. A. Zawadzki, K. Nabeshima, M. Drake, S. Arur *et al.*, 2012 COSA-1 reveals robust homeostasis and separable licensing and reinforcement steps governing meiotic crossovers. Cell 149: 75–87. https://doi.org/10.1016/j.cell.2012.01.052

Zhang, L., K. P. Kim, N. E. Kleckner, and A. Storlazzi, 2011 Meiotic double-strand breaks occur once per pair of (sister) chromatids and, via Mec1/ATR and Tel1/ATM, once per quartet of chromatids. Proc. Natl. Acad. Sci. USA 108: 20036–20041 [corrigenda: Proc. Natl. Acad. Sci. USA 109: 1353 (2012)]. https://doi.org/10.1073/pnas.1117937108

Communicating editor: J. Engebrecht